Space- and time-resolved protein dynamics in single bacterial cells observed on a chip

Dominik Greif[a], Nataliya Pobigaylo[b,1], Benjamin Frage[b], Anke Becker[b], Jan Regtmeier[a,*], Dario Anselmetti[a]

[a] Experimental Biophysics & Applied Nanoscience, Bielefeld University, Universitaetsstr. 25, 33615 Bielefeld, Germany
[b] Institute of Biology III, Faculty of Biology, Albert-Ludwigs-University Freiburg, Schänzlestr. 1, 79104 Freiburg, Germany

ARTICLE INFO

ABSTRACT

Life cell imaging of bacterial cells over long times is very challenging because of the small dimensions and the need for a liquid environment assuring cell viability. In order to obtain space- and time-resolved information about protein dynamics, high resolution time-lapse fluorescence images (TLFI) of single bacterial cells were recorded in a poly(dimethylsiloxane) (PDMS) microfluidic chip. A new gradient coating technique was applied to ensure cell loading. As a proof-of-concept, we monitored the evenly distributed cytoplasmic protein GcrA as well as the asymmetric localization of the DivK protein in cells of *S. meliloti* over at least two division cycles. Localization of DivK was characterized by dividing each bacterial cell into 4 sections with dimensions closely above the optical limit of resolution. This approach of generating spatio-temporal resolved information of protein dynamics in single bacterial cells is applicable to many problems.

1. Introduction

Life cell imaging allows for observations of processes within single cells while they are happening [Stephens and Allan, 2003]. Especially the application of GFP led to great insights into gene expression and protein dynamics. Furthermore, GFP and other autofluorescent proteins serve as reporter proteins visualizing complex protein networks paving the way for systems biology.

There are two important aspects that recently were considered more carefully when discussing single-cell data. Firstly, protein dynamics within single cells is a highly organized process in time and space (reviewed in Thanbichler and Shapiro, 2008). For example, in bacterial cells proteins can asymmetrically localize during cell cycle, e.g. at one pole only. With traditional techniques as real-time PCR, mass spectrometry or flow cytometry, these localizations are not experimentally accessible and such techniques give only static information lacking the temporal dimension.

Secondly, in bulk measurements individual cellular responses are lost as for example temporal variations or cell-to-cell variability. Stochastic nature of gene expression is a central scheme and underlines the importance of studying large ensembles of single cells [Cai et al., 2006; Newman et al., 2006].

Whenever performing life cell imaging, special emphasis should be put on "cells' health on microscope stage" [Stephens and Allan, 2003]. The environment should be as physiological and constant as possible, especially for long-term observations. This includes control of humidity, temperature, gas exchange, and nutrition. As every observation may lead to photo damage, the total amount of added energy should be kept as low as possible.

Additionally, there are some very practical problems: for long-term imaging the cells should be viably immobilized and prevented from dehydration. The standard approach is a sealed pad of agarose that hinders gas exchange and access to the sample.

As a fast-evolving technology, microfluidics allows the processing and manipulation of small amounts of liquids (10^{-9} to 10^{-18} L) using channels with typical dimensions of 10–100 μm [Whitesides, 2006]. Microfluidic cell culture platforms combine the advantages of miniaturization and real-time microscopy allowing culture conditions that are more physiological [Gomez-Sjöberg et al., 2007]. Cells can be studied at single and multi-cellular levels with sin-

---

gle cell resolution and local control of the fluidic environment. The confinement of cells in the chip avoids stacking of cells on top of each other, typically occurring after multiple cell divisions. Therefore, the cells can be identified individually over much longer times compared to traditional time-lapse microscopy without spatial confinement of the cells [Longo and Hasty, 2006]. The possibility for automation promises higher reproducibility, high throughput, more robust systems and the accessibility of faster timescales often limited by the experimenter [El-Ali et al., 2006; Breslauer et al., 2006].

First commercial microfluidic systems are available for life cell imaging, e.g. from Ibidi (plastic gas exchange partially through bottom) or Cellasic (glass bottom; gas permeable PDMS membrane on top). These systems deliver hybrid glass-plastic devices for cell culturing, immobilization and observation. But an adaption of the geometry and the surface chemistry is most often necessary.

With soft lithography new layouts can be created quickly which brings microfluidics to biology focused labs. Microfluidic chip devices are typically fabricated from poly(dimethylsiloxane) (PDMS) involving a process, which requires no cleanroom—once the master replica is fabricated [Xia and Whitesides, 1998]. Additionally, PDMS is compatible with most biological assays; it is transparent, chemically inert and gas permeable. PDMS surfaces can be functionalized with almost the same procedures as glass [Xia and Whitesides, 1998; Merkel et al., 2000].

The literature on applications of microfluidics to cell culture and cell handling is very diverse. An overview of so called micro total analysis system (μTAS) is given by a series of reviews with a special section about cell culture and cell handling [Auroux et al., 2002; Reyes et al., 2002; Vilkner et al., 2004; Dittrich et al., 2006; West et al., 2008]. Microfluidics-based systems biology and cells on chips were recently reviewed [Breslauer et al., 2006; El-Ali et al., 2006] as well as the state of the art concerning the dynamics of single-cell gene expression and appropriate microfluidic techniques [Longo and Hasty, 2006]. Therefore, we only highlight a few examples from the recent literature with direct implications for this study. Gomez-Sjöberg et al. (2007) demonstrated the first fully automated microfluidic cell culture system and applied it to human stem cells. Up to 4 weeks of cell culture were realized with liver cells [Kane et al., 2006]. Sigal et al. (2006) observed protein localizations in human cells and established the *in silico* synchronization of cell division. Survival after antibiotic treatment of a fraction of persistent bacterial cells and their re-growth was investigated in microfluidic devices [Balaban et al., 2004]. Differentiation of muscle cells was observed on a PDMS chip over time spans of 2 weeks [Tourovskaia et al., 2005]. Cookson et al. (2005) observed large numbers of single *S. cerevisiae* cells over many cellular generations in a PDMS device and Megerle et al. (2008) used the commercially available μ-slides from Ibidi to study the arabinose system of *Escherichia coli*. Also PDMS microfluidic devices were used to study gene expression in yeast cells [Ryley and Pereira-Smith, 2006; Charvin et al., 2008].

Microfluidics devices are particularly well suited to study cell cycle processes. Regulation of bacterial cell cycle progression is a fundamental process that is hardly experimentally accessible, mainly because of the small dimensions of the cells. Despite the simplicity of a bacterial cell, studies of the asymmetrical dividing alpha-proteobacterium *Caulobacter crescentus* reveal parallels to the highly organized eukaryotic cell cycle in terms of involvement of DNA methylation, regulated proteolysis and phosphorelays (reviewed in Goley et al., 2009). In *C. crescentus*, cell cycle progression is based on a transcriptional cascade of the three master regulators DnaA, GcrA, and CtrA, cycling out of phase, and driving the expression of cell cycle-regulated genes [Laub et al., 2002; Holtzendorff et al., 2004; Hottes et al., 2005]. A fourth main player, the CcrM

methyltransferase, closes the cell cycle circuit [Collier et al., 2007].

DnaA is an ATPase that binds to the chromosome *replication* origin and initiates replication by unwinding the DNA, enabling the replication complex to start. DnaA also activates the transcription of GcrA, which directly controls the expression of DNA polymerase III holoenzyme, DNA helicase and primase, and about 50 other cell cycle related genes (reviewed in Marinus and Casadesus, 2009). GcrA then activates CtrA, a response regulator driving the expression of about 95 genes, among them genes essential for cell division as well as genes required for polar morphogenesis. At the transcriptional level, CtrA blocks the expression of GcrA, while upregulating its own transcription by induction of a second promoter, resulting in an out of phase oscillation of GcrA and CtrA protein levels. In *C. crescentus*, CtrA-P also silences the origin of replication, thus permitting initiation of DNA replication only once per cell cycle. CtrA is only active when phosphorylated by the CckA-dependent phosphorelay cascade, which is negatively controlled by the essential single domain response regulator DivK [Biondi et al., 2006; Paul et al., 2008]. The transcription of *divK* is induced by CtrA itself, resulting in autoregulation of CtrA.

In this study we investigated the dynamics and localization of GcrA and DivK in *Sinorhizobium meliloti*, a soil bacterium capable of forming a nitrogen-fixing symbiosis with compatible plants of the genera *Medicago*, *Melilotus* and *Trigonella*. In the free-living state, *S. meliloti* cells share the asymmetric cell division with other alpha-proteobacteria [Hallez et al., 2004]. In this study, we present a straightforward disposable microfluidic device fabricated from PDMS and a gradient coating technique that simplifies cell loading and provides different densities of cells.

2. Material and methods

2.1. Construction of DivK and GcrA fusions to fluorescent proteins

The *gcrA* and *divK* coding regions lacking the native stop codon were amplified by PCR using the primer pairs *divK_upstream* (ATATTT<u>GAATTC</u>CGCTCTACGCTGCTGAGTC TC/ATATTT<u>TCTAGA</u>GG<u>CCAGAATGGCC</u>GGCATCGCCCAGATATGTTTT) and *gcrA_upstream* (ATATTT<u>GAATTC</u>ACAAAACCAAGGTTTGCAGGC/ATATTT<u>TCTAG AGG</u><u>CCAGAATGGCC</u>GCGCATGCGCCGGCGCTCGGC) (Restriction sites in the primer sequences are underlined.) and cloned into vector pK19MobSacB [Schäfer et al., 1994] restricted by *Eco*RI and *Xba*I. The downstream primers inserted *Xba*I and *Sfi*I restriction sites downstream of the coding regions.

Downstream regions of *divK* and *gcrA* were amplified using the primer pairs *divK_downstream* (ATATTT<u>TCTAGA</u>GATCGATATGACTGCGCGCAT/ATATTT<u>AAGC TT</u>CCAGTCGAAGCCTC TCCGCAA) and *gcrA_downstream* (ATATTT<u>TCTAGA</u>AGG CCC-CTTTTTTTTTTGCCAT/ATATTT<u>AAGCTT</u>TGTTCCGGGAACTGCTGACCT). The resulting fragments were inserted into the *Xba*I and *Hin*dIII sites of the pK19MobSacB derivates carrying the coding regions.

Universal fluorescent protein gene cassettes were constructed by amplification of the eGFP and mCherry coding regions [Shaner et al., 2004, Clontech] using the primer pair *fp-primer* (ATATTT<u>GAATTC</u>GGCCATTCTGGCCTGATGGTGAGCAAGGGCGAGGAG/ATATTT<u>GGTACC</u>TTACTTGTACAGCTCGTCCAT). The resulting fragments were cloned into the *Eco*RI and *Kpn*I sites of pUC18, inserting a *Sfi*I site upstream of the coding regions. Coding regions of tetracycline (*tet*) or gentamicin (*aacC1*) resistance genes were amplified using the primer pairs *tetA-primer* (ATATTT<u>GGTACC</u>CCTCCTTCGTCGGTGTCGTCG/ATATT <u>TTCTAGA</u>CTCATACCGGCTACG GGAGAC) or *aacC1-primer* (ATATTT<u>GGTACC</u>G GCCGAGGTCTTCCGATCTCC/ATATTT<u>TCTAGA</u>GGGAAGCCGATCTCGGCTTGA) and cloned into the *Kpn*I and *Xba*I sites of pUC18.
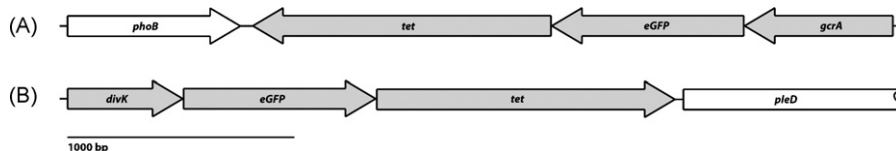
Fig. 1. Constructs of 3′-translational fluorescent fusions integrated into the genome by homologous recombination. (A) *gcrA-eGFP* followed by a tetracycline resistance gene. (B) *divK-eGFP* followed by a tetracycline resistance gene.
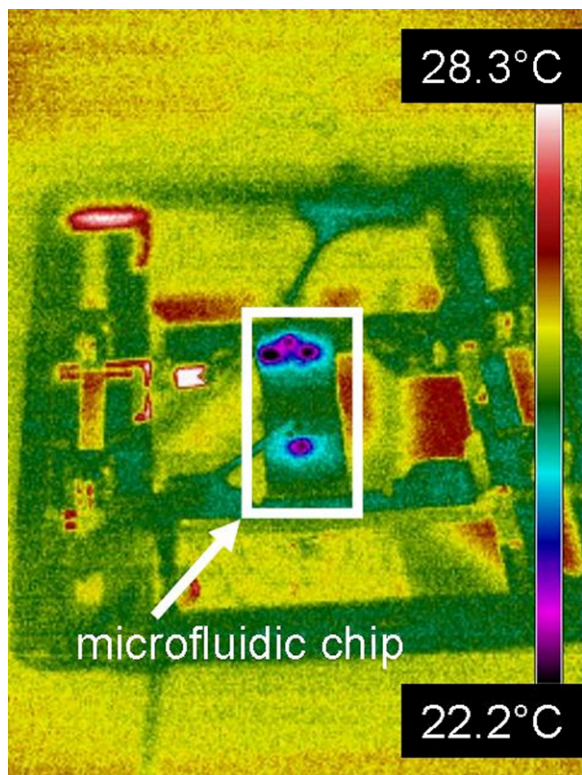
Fig. 2. IR image of the microfluidic chip on the *x–y*-stage at room temperature (25 °C): The white rectangle indicates the chip, which displays the same temperature as the room with exceptions at the reservoirs. There, water evaporates cooling the surface of the liquid drop.

Combination of both fragment types resulted in eGFP-*tet* or mCherry-*aacC1* cassettes that were inserted into the *Sfi*I and *Xba*I sites of pK19MobSacB derivates carrying coding and downstream regions of *divK* or *gcrA* generating 3′-translational fusions of *divK* or *gcrA* to the eGFP or mCherry fluorescent protein genes followed by the antibiotic resistance gene and the downstream fragment (Fig. 1).

These constructs were transferred by *E. coli* S17-1 mediated conjugation [Simon, 1984] to *S. meliloti* and integrated into the chromosome by homologous recombination replacing the native genes. The resulting strains carried *divK*-eGFP-*tet*, *gcrA*-eGFP-*tet*, or *gcrA*-mCherry-*aacC1* fusions as single copies at the native loci in the chromosome.

2.2. Time-lapse life cell imaging

All chemicals and reagents were obtained from Sigma–Aldrich (Germany). The microfluidic chips were fabricated by soft lithography [Xia and Whitesides, 1998]. Briefly (see also references Regtmeier et al., 2007; Greif et al., 2008), the masterwafer was lithographically patterned with the photoresist SU8-5 (Micro Resist Technology, Germany) and processed as indicated by the manufacturer. Poly(dimethylsiloxane) was obtained from Dow Corning, USA. Polymer and linker were mixed 10:1 and poured over the masterwafer. The polymer was cured at 85 °C for 4 h, peeled off the wafer and cut with a scalpel. Reservoir holes (3 mm diameter) were punched and the PDMS slabs were consecutively cleaned in acetone, ethanol and water in an ultrasonic bath (Elma T 490 DH, Germany). The same cleaning procedure was applied to the glass cover slips (Menzel, Germany). After drying with nitrogen (Linde, Germany), the glass slides and the PDMS slabs were exposed to oxygen plasma for 30 s (home-built plasma chamber; 50 kV, 500 kHz Tesla coil with an electrode distance of 6.1 cm and 10^{-1} mbar) and assembled shortly after plasma treatment. The chip reservoirs were enlarged by putting small pieces of PDMS also with holes on top of the reservoirs resulting in ~30 μL volume per reservoir. After at least 1 h the chips were filled with a polyethylenimine (PEI, M_n ~ 60,000, M_w 750,000) coating in MilliQ-H_2O (Millipore, USA) (concentration 0.1%). Therefore, one reservoir of the linear channel (length: 1 cm, height: 3 μm, width: 450 μm) was filled with 14 μL MilliQ-H_2O and then the other reservoir was filled with 15 μL PEI coating. After 5 min the PEI coating solution was removed, the reservoirs and the channels were washed with MilliQ-H_2O and afterwards filled with Vincent minimal medium (VMM, 1 mM MgSO$_4$, 18.7 mM NH$_4$Cl, 10 mM Na$_2$ succinate, 456 μM CaCl$_2$, 35 μM FeCl$_3$, 4 μM biotin, 48.5 μM H$_3$BO$_3$, 10 μM MnSO$_4$, 1 μM ZnSO$_4$, 0.5 μM CuSO$_4$, 0.27 μM CoCl$_2$, 0.5 μM NaMoO$_4$) [Vincent, 1970] for the measurements (see Sections 3 and 4).

The *S. meliloti* cells were grown at 28 °C in liquid cultures with Vincent minimal medium overnight to an approximate O.D.$_{580}$ of ~0.6–0.8.

Before loading, the cells were washed with VMM and then loaded onto the chip by hydrodynamic pressure from the reser-
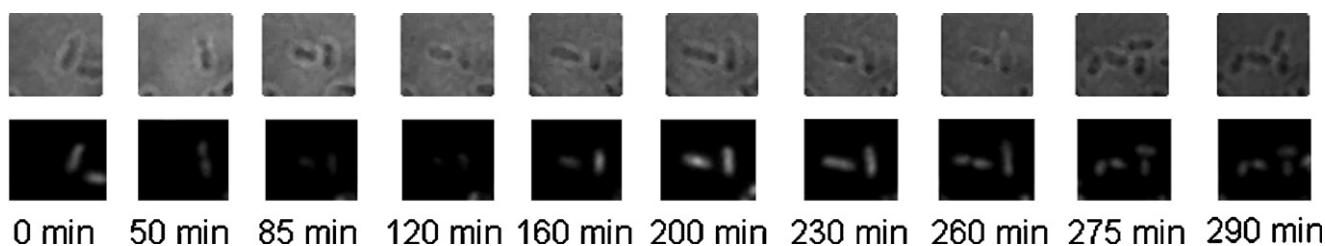
Fig. 3. Time-lapse brightfield (top row) and fluorescence (bottom row) images of *S. meliloti* bacterial cells carrying the fusion protein GcrA-EGFP (RT = 27.6 ± 0.4 °C). The cell divides twice during the time of observation. An oscillation of the fluorescence intensity can be observed.
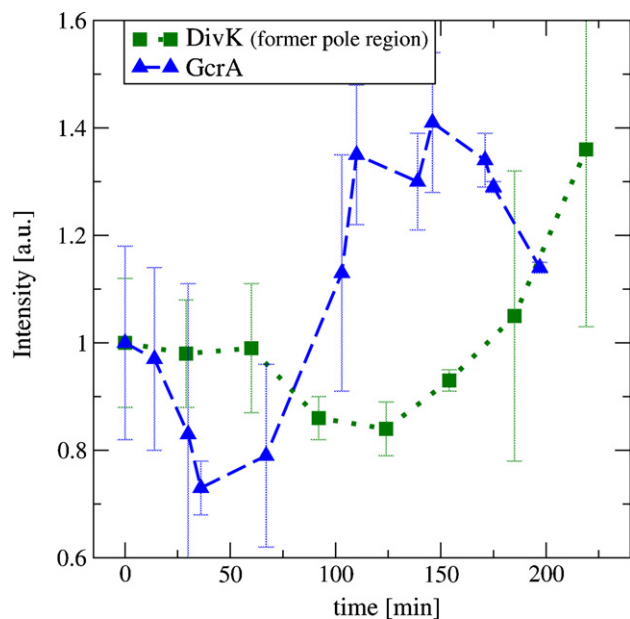
Fig. 4. Temporal protein dynamics of GcrA-eGFP ($n = 4$ complete cell cycles observed) and DivK-eGFP (former pole region only (section 1); see also Fig. 7) ($n = 2$ complete cell cycles observed; including images before and after the completed cycle, an average of 4 images per data point were used); normalized fluorescence intensity over an ensemble of *in silico* synchronized *S. meliloti* cells. Time zero corresponds to the first images after cell division. All intensities were normalized to one for time zero for better comparability.

voir that was initially filled with MilliQ-H_2O during the coating procedure. Depending on the PEI concentration, the cells were electrostatically bound to the surface within the microchannel before observation.

Brightfield and fluorescence microscopy were performed on an inverted microscope (Axiovert 200 Zeiss Germany) equipped with a motorized stage (Ludl) a mercury arc lamp (HBO 100 Zeiss) in addition to the microscope incident light, a 100× oil immersion objective (Plan Neofluar, NA 1.3, Zeiss, Germany), a sensitive CCD camera (Imager 3LS; LaVision, Germany; identical with Sensicam from PCO) and the corresponding grabber card for acquiring images from the camera. A grey filter (transmittance 30%) in the excitation light beam and two different fluorescence filter sets (Fs 44, Fs 20, Zeiss, Germany) were used for observation of eGFP and mCherry fusion proteins. DaVis 6.2 was used for image acquisition with exposure times of 500 ms for the DivK-eGFP fusion constructs and 250 ms for the GcrA-eGFP and full resolution of the CCD chip (1280 × 1024 pixels). In order to minimize optical drift, the laboratory was heated to 28 °C for at least one night before observation. The temperature of the microfluidic chip was checked with an IR camera (ThermaCAM E320, FLIR Systems).

A brightfield and a fluorescence image of the growing cells were taken about every 30 min, keeping the light exposure times as short as possible. Every hour the level of filling of the reservoirs was checked and filled up if necessary with MilliQ-H_2O water to keep the salt concentration and thus the osmotic pressure nearly constant.

ImageJ (1.41o) was used for image postprocessing and data analysis. Every cell dividing at least two times was analysed based on the fluorescence intensity of the expressed fusion protein. For GcrA, the mean fluorescence intensity over the whole cell was determined. The same was done for DivK, but additionally every cell was divided into 4 equidistant sections (see Fig. 7) and the intensity of the brightest pixel in each section was recorded.

Cell synchronization was performed *a posteriori* [Sigal et al., 2006]. Because only cells dividing twice were analysed, at least one

full cell cycle was observed. The time point of the first division (first image after cell division) was taken as time zero and the observed fluorescence intensities were averaged for several cells. For GcrA, the fluorescence intensity was normalized to one for time zero. For DivK, the observed intensity of the brightest pixel in each section was normalized by the mean intensity of the whole cell. This representation allows discrimination whether there is a locally confined increase in fluorescence intensity or an increase that extends over the full cell.

2.3. Scanning electron microscopy

For scanning electron microscopy glass slides (Menzel, Germany) were cleaned in an ultrasonic bath (Elma T 490DH), consecutively in acetone, ethanol and in MilliQ-H_2O for 20 s each and afterwards dried with nitrogen. Cells from 1 mL bacterial overnight cultures in VMM medium were centrifuged (5 min at 1500 rpm, Eppendorf centrifuge S417C) and washed twice with PBS (phosphate buffered saline, Fluka). Finally, the pellet was resuspended in 500 µL PBS buffer. Washing was followed by fixation of the cells in 1.5% paraformaldehyde and 1.5% glutaraldehyde in PBS for 1 h at room temperature (RT). Afterwards the cells were washed again and resuspended in MilliQ-H_2O. For dehydration the water in the sample was slowly exchanged over at least 48 h against ethanol. Then after centrifugation (5 min at 1500 rpm) the ethanol was wasted and the pellet resuspended in 500 µL isopropanol. For drying, 10 µL and 20 µL of each sample were dropped onto 8 mm × 8 mm glass slides and dried in an isopropanol saturated atmosphere over at least 48 h at RT. For imaging the bacterial samples, gold-layers of 12 nm thickness were applied by sputtering (BAL TEC MED 020 coating system) before they were transferred into the scanning electron microscope (JEOL JSM-880).

3. Results

3.1. Conditions for cell growth on the microfludic chip device

Cell viability is one crucial aspect when performing long-term life cell imaging. The optimal growth temperature of *S. meliloti* is in the range of 28–30 °C. Therefore, we first validated with an infrared (IR) camera that the microfluidic chip had the intended temperature on the microscope stage. Comparison of the temperature of the microfluidic chip determined from IR images with room temperature revealed a very good agreement, thus room temperature sufficiently characterized the chip temperature. An example of such an IR image is shown in Fig. 2. *S. meliloti* cells divided about every three hours on the chip, which is comparable to the generation time during the exponential growth phase in regular liquid cultures [Adt et al., 2000]. This confirms optimal cell viability and a regular division time on the chip.

3.2. Time-lapse studies of GcrA and DivK protein dynamics and localization in S. meliloti

For a proof-of-concept, GcrA and DivK of *S. meliloti* were chosen because they have close homologues implicated in regulating the cell cycle in *C. crescentus*, a well studied model organism for this process [Holtzendorff et al., 2004; Sommer and Newton, 1991]. The wild-type gene was replaced by a C-terminal fusion of eGFP to either GcrA or DivK, or of mCherry to GcrA (see Fig. 1). Replacement of the wild-type copy resulted in a single copy of the *gcrA-eGFP, gcrA-mCherry*, or *divK-eGFP* constructs at the native locus in the genome and in expression of these fusion constructs driven by the native promoters. In *C. crescentus* GcrA was shown to be an important master regulator of cell cycle progression [Holtzendorff et al.,
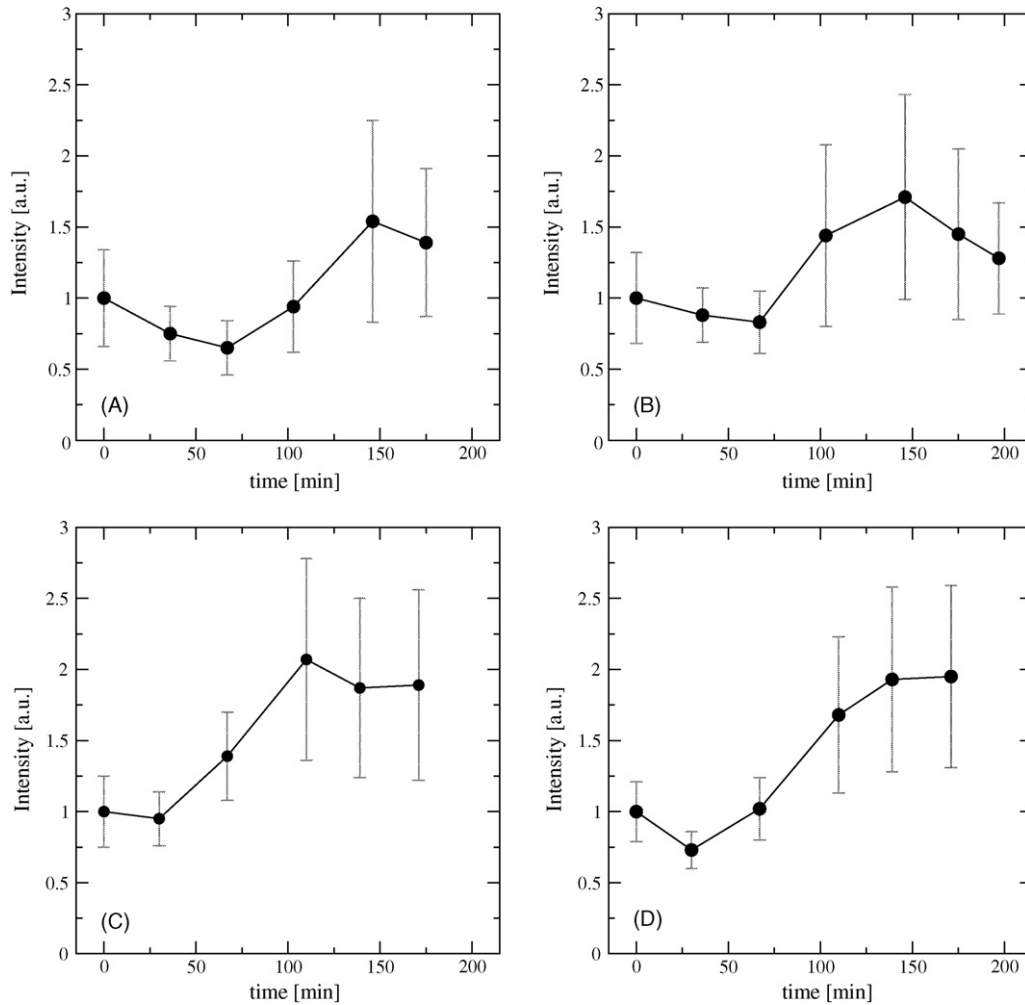
Fig. 5. Temporal protein dynamics of GcrA-eGFP over one complete cell cycle in single cells. Time zero corresponds to the first image after cell division; intensity was normalized to one for time zero (error bars = standard deviation of the fluorescence intensity). The plots shown in (A and B) as well as those in (C and D) belong to daughter cells originated from the same mother cells.

2004] implying that the *S. meliloti* orthologue has a similar function in the control of the cell cycle. Overexpression of *divK* in *S. meliloti* resulted in inhibition of the cell division [Lam et al., 2003] demonstrating that the strength and time pattern of *divK* expression is critical. Replacement of the wild-type copy of *gcrA* or *divK* by the fluorescent fusion construct resulted in viable strains which did not differ from the wild-type in terms of morphology and generation time. Growth of cells carrying the fusion constructs was comparable to that of the wild-type strain. In our setup, the doubling time of *S. meliloti* was about 200 min. This indicates that the fusion constructs were functional.

When interpreting acquired images, the signal to noise ratio (S/N) is critical especially for low fluorescence intensity. As the fluorescence signal of the observed proteins oscillate in time, a minimum and a maximum value of the S/N ratio were calculated. The best S/N for the GcrA-eGFP construct was 27.8, the worst 9.6; for the DivK-eGFP mutant 36.8 and 22.1 were determined, respectively. Hence, a clear distinction between fluorescence signal and background is achieved even when the fluorescence intensity is low (a S/N of 3 is commonly assumed to be sufficient).

Time-lapse brightfield and fluorescence images (TLFI) were recorded over a time span of about 6 h of bacteria expressing the fusion proteins. GcrA-GFP was expressed in a cell cycle dependent oscillation pattern. A typical set of TLFI images of GcrA-eGFP is shown in Fig. 3. A single bacterial cell divided twice during the time of observation. The visual impression of the TLFI images suggests
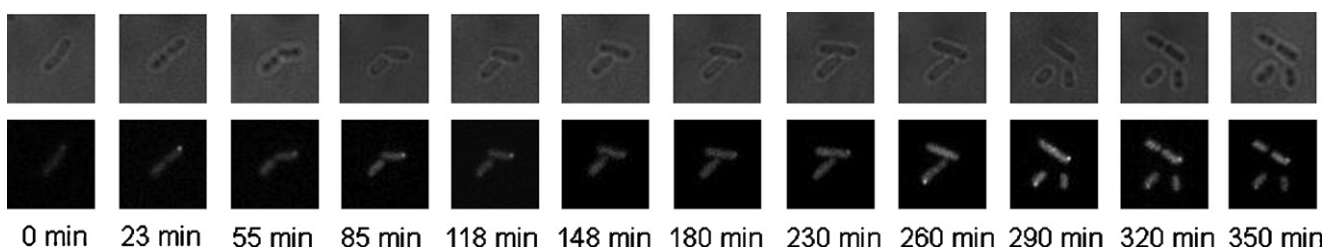
Fig. 6. Time-lapse brightfield (top row) and fluorescence (bottom row) images of cells carrying the fusion protein DivK-EGFP (RT = 28.2 ± 0.3 °C). The cell divides twice during the time of observation. For example, asymmetric localizations of DivK can be clearly observed at 23 and 290 min in the former pole regions of the bacteria.

an oscillation in the overall fluorescence intensity, corresponding to oscillation of protein concentration. This was quantified as shown in Fig. 4 (blue triangles). About 50 min after cell division, the fluorescence intensity reaches the minimum, about 0.7-fold of the intensity at time 0. GcrA then accumulates to a maximum of 1.4-fold at 100 min, and starts to decay slowly about 50 min later. In order to allow a more detailed interpretation of Fig. 4 and to address cell-to-cell variability, the fluorescence intensity is plotted for single cells in Fig. 5. Here the curves shown in (A) and (B) as well as those shown in (C) and (D) belong to daughter cells originated from the same mother cells.

Generally, locations of proteins within the cell (especially within small bacteria) and their temporal dynamics are hard to detect with traditional techniques. Therefore, TLFI images of the fusion protein DivK-eGFP were taken. One time series is shown in Fig. 6. Bright spots were observed at a pole region at some time points during the cell cycle. For a more detailed analysis, every cell was sectioned into 4 regions (see Fig. 7). Herein, region 1 corresponds to the former pole region and section 4 to the new pole region.

In Fig. 8A and B the development of the fluorescent intensity over time is depicted for each section of individual daughter cells descending from the same mother cell. Right after cytokinesis DivK was distributed in an asymmetrical fashion in the daughter cells. This difference in morphology of the two types of daughter cells is exemplified in Fig. 8. Fluorescence intensities of the smaller and larger daughter cells denote variances in DivK localization. The larger daughter cell harboured DivK localized at the pole opposite to the former site of cell division. Here, as cell growth progressed, DivK was released from the pole, and evenly distributed. Just before cell division, DivK accumulated again at the same pole. In the smaller daughter cell, DivK was uniformly distributed over almost the entire cell cycle, but localized and increased at its old pole rapidly just before cell division. At this time, the mean fluorescence intensity at the old pole revealed a 2-fold increase of protein content. Interestingly, in Fig. 6 the smaller cell divided faster than the larger cell, which is unusual for *S. meliloti* [Lam et al., 2003]. After the second cell division, the two resulting daughter cells showed a similar asymmetric distribution of DivK, with localization in the larger cell, but evenly dispersed DivK in the smaller cell.

In Fig. 8C and D the observed fluorescence intensity for a double fusion construct is depicted. This strain carried simultaneously the fusion proteins DivK-eGFP and GcrA-mCherry, in which only the eGFP was excited and observed with the corresponding filter set. Obviously, the time of the cell cycle was about doubled. Possible reasons could be that the two fusion proteins might function slightly worse, e.g. due to minor changes in protein folding, as compared to the wild-type proteins and that the accumulation of changes led to the prolonged cell division time. However, the basic functionality is maintained, as the qualitative spatio-temporal dynamics are preserved in comparison to Fig. 8A and B, showing the behaviour of cells carrying only a single fusion protein. Furthermore, no morphological differences were observed between wild-type cells, cells carrying only a single fusion construct, or both constructs.

In Fig. 4, the spatio-temporal dynamics of DivK and GcrA are summarized. Because of the asymmetric localization of DivK, only the former pole region is shown (see also Fig. 8).

4. Discussion

4.1. Microfluidic chips in cell biology

The microfluidic chip proved beneficial as a defined and controllable liquid environment that assures cell viability. The height
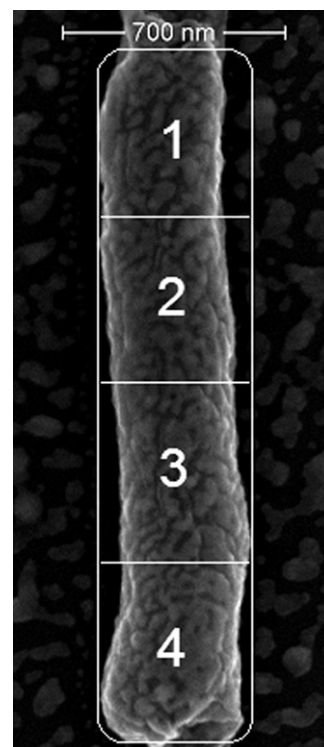
Fig. 7. Scanning electron image of *S. meliloti* with sections used for data analysis. The observed wild-type cell has a width of about 0.4 μm and a length of about 2 μm. The protrusions on the cell surface are not caused by sample preparation but can also be found less pronounced on living *S. meliloti* cell envelopes imaged with AFM in the liquid phase [Greif et al., 2010].

of the device was chosen such that cell stacking was avoided. It further reduced the fluorescence background as only a small volume of the culture medium contributes to the fluorescence signal. The cell viability was not interfered by the small volume of medium as the division times demonstrate. This can be attributed to the biocompatibility and gas permeability of the used elastomer assuring a sufficient oxygen supply. The gas permeability was determined to be 245×10^{-10} cm^3(STP) cm/cm^2 s cm Hg [Singh et al., 1998]. The applied gradient coating technique further underlines the advantages of miniaturization. It allows for a distinct flow control and therefore a spatially controlled application of the surface coating. This makes a region dependent density of adhered cells possible. Cell density is critical especially for long observation times, as the individual cells must remain distinguishable despite cell multiplication. At the same time enough cells in the field of view are necessary to allow a substantiated data analysis.

4.2. Technical interpretation of obtained spatio-temporal information

As depicted in the SEM image in Fig. 7, the typical cell width is only about 400 nm and a length of about 1.5–3 μm. The Rayleigh criterion limits the resolution of classical optical microscopy to about half the wavelength. Using light emission at about 530 nm, the smallest theoretically distinguishable features have to be 200 nm apart with a numerical aperture of 1.3 of the objective [Hecht and Zajac, 2003]. This stresses the difficulty but also the theoretical feasibility of space resolved (classical) fluorescence microscopy of single bacterial cells. The number of cell sections was chosen accordingly, thus they have a minimum length of about 300 nm (directly after cell division increasing to about 800 nm shortly before cell division). Nevertheless, an oversampling was used, i.e.
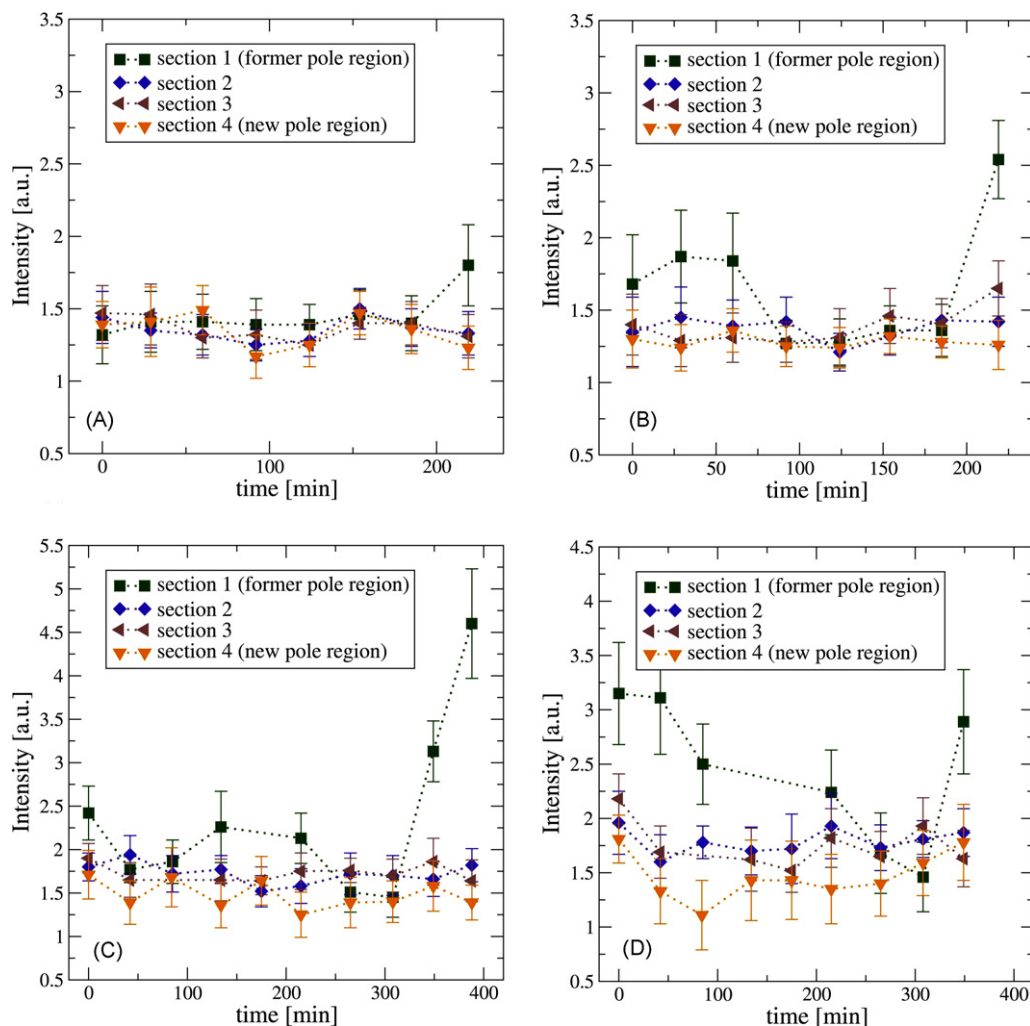
Fig. 8. Asymmetric spatial and temporal dynamics of DivK-eGFP over one cell cycle in single cells originating from same mother cells for the four regions indicated in Fig. 7. Time zero corresponds to the first image after cell division (error bars = standard deviation of the fluorescence intensity). Smaller (A) and larger (B) daughter cell of DivK-eGFP single translational fusion. Smaller (C) and larger (D) daughter cell of DivK-eGFP, GcrA-mCherry double fusion, only DivK-eGFP observed.

one pixel on the CCD camera corresponded to 67 nm, easing image analysis while the physical limit of resolution is still valid.

The large S/N ratios stated in the results section suggest that the error bars observed in Fig. 4 are not due to a lack of S/N ratio. More likely, the large error bars can be attributed to the heterogeneity of single cells [Cai et al., 2006; Newman et al., 2006], which may be due to different levels of expressed proteins, e.g. caused by different uptake of nutrients resulting in deviations in cell growth and variation in gene expression. When studying alpha-proteobacteria, the most prominent factor of heterogeneity is their asymmetrical division, as denoted in Fig. 8. Complete characterization of protein localizations would require discrimination of the two types of daughter cells with sufficient replicates. An additional reason for the observed heterogeneity might be induced photo damage. Every time the cells are imaged, they are exposed to light (475 nm) and the eGFP is excited. In order to minimize potential damage, exposure times and light intensity were optimised prior image acquisition and kept constant but as short and low as possible. However, no difference was observed in division times on the chip compared to conventional cell culture providing no evidence for photo damage.

4.3. Biological interpretation and comparison to C. crescentus

In this study we investigated dynamics and localization of GcrA and DivK involved in cell cycle control of *S. meliloti*. Both proteins have been previously analysed in detail in *C. crescentus*, a model organism for bacterial cell cycle studies [Holtzendorff et al., 2006; Jacobs et al., 2001].

Alpha-proteobacteria divide asymmetrically, producing two genetic identical daughter cells of distinct morphology. In *C. crescentus*, the bigger stalked cell can immediately enter the prokaryotic S phase and reinitiate chromosome replication and cytokinesis, whereas the smaller swarmer cell stays in the G1 phase for about 30 min prior to differentiation into a stalked cell. This asymmetric regulation is mediated by the spatial and temporal localization of phosphorylated DivK [Paul et al., 2008]. In swarmer cells, DivK is dispersed and inactivated by its phosphatase PleC. Here, CtrA is phosphorylated and active, blocking the origin of replication. In stalked cells, DivK is localized and activated at the pole by its membrane associated histidine kinase DivJ. DivK-P inactivates CtrA by blocking the CckA phosphorelay, and initiation of DNA replication begins.

The *S. meliloti* DivK homologue has previously been described by [Lam et al., 2003]. smDivK complemented a *C. crescentus* DivK mutant, demonstrating that the *S. meliloti* DivK is functional in this organism. Our time-lapse analyses of GFP-tagged DivK support the results of [Lam et al., 2003], showing a localization pattern different from the behaviour of DivK in *C. crescentus*. In both daughter cells the intensity is increasing at only one pole at the end of the cell cycle, in contrast to the bipolar localization in *C. crescentus*. DivK

is active only in its phosphorylated form, and phosphorylation is coupled with the location at a pole [Lam et al., 2003]. In *C. crescentus*, active DivK-P promotes clearing of CtrA at the old cell pole [McAdams and Shapiro, 2003]. This degradation of CtrA is required for replication initiation and contributes to only one round of replication per cell cycle [Collier et al., 2007]. In *S. meliloti*, chromosome replication also happens only once per cell cycle. The unipolar localization of smDivK at the old pole suggests differences in the CtrA phosphorelay cascade. These differences in polar morphology, but shared asymmetrical division between these two species suggest a conserved main mechanism in control of the cell cycle [McAdams et al., 2004] in alpha-proteobacteria, with adjustments to different conditions of live.

TLFI of *S. meliloti* cells carrying translational eGFP fusions to the main cell cycle regulator GcrA showed oscillation of protein content over the course of the cell cycle. Since *S. meliloti* cells were not synchronized, *in silico* synchronization [Sigal et al., 2006] of single cell fluorescent intensity was performed. The acquisition of cell cycle dependent protein expression data using GFP-tagged proteins differs from traditional methods, e.g. western blots of a synchronized culture. Factors to debate when interpreting this data may include fluorescent protein activation, half-life, or degradation time varying from the protein of interest. Our data suggests a profile of the *S. meliloti* GcrA ortholog similar to that of the *C. crescentus* GcrA. Comparing the *S. meliloti* GcrA-eGFP profile to the GcrA protein content of synchronized *C. crescentus, de novo* accumulation of smGcrA seems to start later in the cell cycle. Second, a notable difference is the presence of smGcrA at the beginning of the cell cycle in both types of daughter cells, decreasing in the first 40 min. In *C. crescentus* swarmer cells, active CtrA blocks DNA replication and represses transcription of GcrA [Collier et al., 2006]. smGcrA being present in *S. meliloti* small daughter cells may suggest slightly different functions of the conserved main cell cycle regulators GcrA and CtrA.

5. Conclusions

A PDMS microfluidic chip was used for time-lapse fluorescence imaging (TLFI) of single bacterial cells. It assures cell viability and allows for the spatially controlled application of a surface coating. With this approach cells could viably be immobilized with tailored densities. The design of the device avoids cell stacking and therefore allows for cell tracking over many hours. Despite the small size of the bacterial cells, time *and* space resolved protein dynamics could be observed for two proteins involved in cell cycle regulation in single bacterial cells of *S. meliloti*. The localization pattern characterization of proteins was achieved by dividing the cell into four sections. The spatial extension of each section was just above the limit of (classical) optical microscopy. The obtained information revealed new insights into the dynamics of proteins related to cell cycle control of *S. meliloti* and interesting analogies to *C. crescentus*.

Acknowledgements

References

Adt, I., Courtois, B., Courtois, J., 2000. Increase of the ATP-dependent phosphoenolpyruvate carboxykinase activity in *Sinorhizobium meliloti* during hypothermic environmental conditions. Int. J. Food Microbiol. 55, 69–72.

Auroux, P.-A., Iossifidis, D., Reyes, D.R., Manz, A., 2002. Micro total analysis systems. 2. Analytical standard operations and applications. Anal. Chem. 74, 2637–2652.

Balaban, N.Q., Merrin, J., Chait, R., Kowalik, L., Leibler, S., 2004. Bacterial persistence as a phenotypic switch. Science 305, 1622–1625.

Biondi, E.G., Reisinger, S.J., Skerker, J.M., Arif, M., Perchuk, B.S., Ryan, K.R., Laub, M.T., 2006. Regulation of the bacterial cell cycle by an integrated genetic circuit. Nature 444, 899–904.

Breslauer, D.N., Lee, P.J., Lee, L.P., 2006. Microfluidics-based systems biology. Mol. BioSyst. 2, 97–112.

Cai, L., Friedman, N., Xie, X.S., 2006. Stochastic protein expression in individual cells at the single molecule level. Nature 440, 358–362.

Charvin, G., Cross, F.R., Siggia, E.D., 2008. A microfluidic device for temporally controlled gene expression and long-term fluorescent imaging in unperturbed dividing yeast cells. PLoS e1268, 1–12.

Collier, J., Murray, S.R., Shapiro, L., 2006. DnaA couples DNA replication and the expression of two cell cycle master regulators. EMBO J. 25, 346–356.

Collier, J., McAdams, H.H., Shapiro, L., 2007. A DNA methylation ratchet governs progression through a bacterial cell cycle. Proc. Natl. Acad. Sci. U.S.A. 104, 17111–17116.

Cookson, S., Ostroff, N., Pang, W.L., Volfson, D., Hasty, J., 2005. Monitoring dynamics of single-cell gene expression over multiple cell cycles. Mol. Syst. Biol., 1–6, doi:10.1038/msb4100032.

Dittrich, P., Tachikawa, K., Manz, A., 2006. Micro total analysis systems. Latest advancements and trends. Anal. Chem. 78, 3887–3908.

El-Ali, J., Sorger, P.K., Jensen, K., 2006. Cells on chips. Nature 442, 403–411.

Goley, E.D., Toro, E., McAdams, H.H., Shapiro, L., 2009. Dynamic chromosome organization and protein localization coordinate the regulatory circuitry that drives the bacterial cell cycle. Cold Spring Harb Symp Quant Biol. 74, 55–64.

Gomez-Sjöberg, R., Leyrat, A.A., Pirone, D.M., Chen, C.S., R: Quake, S., 2007. Versatile, fully automated, microfluidic cell culture system. Anal. Chem. 79, 8557–8563.

Greif, D., Wesner D., Regtmeier, J., Anselmetti, D., 2010. High resolution imaging of surface patterns of single bacterial cells. Ultramicroscopy. doi:10.1016/j.ultramic.2010.06.004.

Greif, D., Galla, L., Ros, A., Anselmetti, D., 2008. Single cell analysis in full body quartz glass chips with native UV-laser induced fluorescence detection. J. Chromatogr. A 1206 (1), 83–88.

Hallez, R., Bellefontaine, A.-F., Letesson, J.-J., De Bolle, X., 2004. Morphological and functional asymmetry in alpha-proteobacteria. Trends Microbiol. 12 (8), 36136–36145.

Hecht, E., Zajac, A., 2003. Optics, 4th ed., International ed. Addison-Wesley Longman, Amsterdam.

Holtzendorff, J., Hung, D., Brende, P., Reisenauer, A., Viollier, P.H., McAdams, H.H., Shapiro, L., 2004. Oscillating global regulators control the genetic circuit driving a bacterial cell cycle. Science 304, 983–987.

Holtzendorff, J., Reinhardt, J., Viollier, P.H., 2006. Cell cycle control by oscillating regulatory proteins in *Caulobacter crescentus*. Bioessays 28, 355–361.

Hottes, A.K., Shapiro, L., McAdams, H.H., 2005. DnaA coordinates replication initiation and cell cycle transcription in *Caulobacter crescentus*. Mol. Microbiol. 58, 1340–1353.

Jacobs, C., Hung, D., Shapiro, L., 2001. Dynamic localization of a cytoplasmic signal transduction response regulator controls morphogenesis during the Caulobacter cell cycle. Proc. Natl. Acad. Sci. U.S.A. 98, 4095–4100.

Kane, B.J., Zinner, M.J., Yarmush, M.L., Toner, M., 2006. Liver-specific functional studies in a microfluidic array of primary mammalian hepatocytes. Anal. Chem. 78, 4291–4298.

Lam, H., Matroule, J.Y., Jacobs-Wagner, C., 2003. The asymmetric spatial distribution of bacterial signal transduction proteins coordinates cell cycle events. Dev. Cell 5, 149–159.

Laub, M.T., Chen, S.L., Shapiro, L., McAdams, H.H., 2002. Genes directly controlled by CtrA, a master regulator of the Caulobacter cell cycle. Proc. Natl. Acad. Sci. U.S.A. 99, 4632–4637.

Longo, D., Hasty, J., 2006. Dynamics of single-cell gene expression. Mol Sys Biol, 1–10, doi:10.1038/msb4100110.

Marinus, M.G., Casadesus, J., 2009. Roles of DNA adenine methylation in host-pathogen interactions: mismatch repair, transcriptional regulation, and more. FEMS Microbiol. Rev. 33, 488–503.

McAdams, H.H., Shapiro, L., 2003. A bacterial cell-cycle regulatory network operating in time and space. Science 301 (5641), 1874–1877.

McAdams, H.H., Srinivasan, B., Arkin, A.P., 2004. The evolution of genetic regulatory systems in bacteria. Nat. Rev. Genet. 5, 169–178.

Megerle, J.A., Fritz, G., Gerland, U., Jung, K., Rädler, J.O., 2008. Timing and dynamics of single cell gene expression in the Arabinose utilization system. Biophys. J. 95, 2103–2115.

Merkel, T.C., Bondar, V.I., Nagai, K., Freeman, B.D., Pinnau, I., 2000. Gas sorption, diffusion, and permeation in poly(dimethylsiloxane). J. Polym. Sci. 38, 415–434.

Newman, J.R.S., Ghaemmaghami, S., Ihmels, J., Breslow, D.K., Noble, M., DeRisi, J.L., Weissman, J.S., 2006. Single-cell proteomic analysis of *S. Cerevisiae* reveals the architecture of biological noise. Nature 441, 840–846.

Paul, R., Jaeger, T., Abel, S., Wiederkehr, I., Folcher, M., Biondi, E.G., Laub, M.T., Jenal, U., 2008. Allosteric regulation of histidine kinases by their cognate response regulator determines cell fate. Cell 133, 452–461.

Regtmeier, J., Duong, T.T., Eichhorn, R., Anselmetti, D., Ros, A., 2007. Dielectrophoretic manipulation of DNA: separation and polarizability. Anal. Chem. 79, 3925–3932.

Reyes, D.R., Iossifidis, D., Auroux, P.-A., Manz, A., 2002. Micro total analysis systems. 1. Introduction, theory and technology. Anal. Chem. 74, 2623–2636.

Ryley, J., Pereira-Smith, O.M., 2006. Microfluidics device for single cell gene expression analysis in *Saccharomyces cerevisiae*. Yeast 23, 1065–1073.

Schäfer, A., Tauch, A., Jäger, W., Kalinowski, J., Thierbach, G., Pühler, A., 1994. Small mobilizable multi-purpose cloning vectors derived from the *Escherichia coli* plasmids pK18 and pK19: selection of defined deletions in the chromosome of *Corynebacterium glutamicum*. Gene 145, 69–73.

Shaner, N.C., Campbell, R.E., Steinbach, P.A., Giepmans, B.N., Palmer, A.E., Tsien, R.Y., 2004. Improved monomeric red, orange and yellow fluorescent proteins derived from Discosoma sp. red fluorescent protein. Nat. Biotechnol. 22, 1567–1572.

Sigal, A., Milo, R., Cohen, A., Geva-Zatorsky, N., Klein, Y., Alaluf, I., Swerdlin, N., Perzov, N., Danon, T., Liron, Y., Raveh, T., Carpenter, A.E., Lahav, G., Alon, U., 2006. Dynamic proteomics in individual human cells uncovers widespread cell-cycle dependence of nuclear protins. Nat. Meth. 3, 525–531.

Simon, R., 1984. High frequency mobilization of gram-negative bacterial replicons by the in vitro constructed Tn5-Mob transposon. Mol. Gen. Genet 196, 413–420.

Singh, A., Freeman, B.D., Pinnau, I., 1998. Pure and mixed gas acetone/nitrogen permeation properties of polydimethylsiloxane [PDMS]. J. Polym. Sci. B 36, 289–301.

Sommer, J.M., Newton, A., 1991. Pseudoreversion analysis indicates a direct role of cell division genes in polar morphogenesis and differentiation in *Caulobacter crescentus*. Genetics 129, 623–630.

Stephens, D.J., Allan, V.J., 2003. Light microscopy techniques for live cell imaging. Science 300, 82–86.

Thanbichler, M., Shapiro, L., 2008. Getting organized—how bacterial cells move proteins and DNA. Nat. Rev. Microbiol. 6, 28–40.

Tourovskaia, A., Figueroa-Masot, X., Folch, A., 2005. Differentiation-on-a-chip: a microfluidic platform for long-term cell culture studies. Lab Chip 5, 14–19.

Vilkner, T., Janasek, D., Manz, A., 2004. Micro total analysis systems. Recent developments. Anal. Chem. 76, 3373–3386.

Vincent, J.M., 1970. A Manual for the Practical Study of the Root-Nodule Bacteria. International Biological Program Handbook, vol. 15. Blackwell Scientific Publications, Oxford, England.

West, J., Becker, M., Tombrink, S., Manz, A., 2008. Micro total analysis systems: latest achievements. Anal. Chem. 80, 4403–4419.

Whitesides, G.M., 2006. The origins and the future of microfluidics. Nature 442, 368–373.

Xia, Y., Whitesides, G.M., 1998. Soft lithography. Angew. Chem. Int. Ed. 37, 550–575.